

Two atomic constraints unambiguously position the S4 segment relative to S1 and S2 segments in the closed state of Shaker K channel

Fabiana V. Campos, Baron Chanda, Benoît Roux, and Francisco Bezanilla

PNAS published online Apr 30, 2007;
doi:10.1073/pnas.0702638104

This information is current as of May 2007.

Supplementary Material

Supplementary material can be found at:
www.pnas.org/cgi/content/full/0702638104/DC1

This article has been cited by other articles:
www.pnas.org#otherarticles

E-mail Alerts

Receive free email alerts when new articles cite this article - sign up in the box at the top right corner of the article or [click here](#).

Rights & Permissions

To reproduce this article in part (figures, tables) or in entirety, see:
www.pnas.org/misc/rightperm.shtml

Reprints

To order reprints, see:
www.pnas.org/misc/reprints.shtml

Notes:

Two atomic constraints unambiguously position the S4 segment relative to S1 and S2 segments in the closed state of Shaker K channel

Fabiana V. Campos*, Baron Chanda†, Benoît Roux*, and Francisco Bezanilla*‡

*Institute for Molecular Pediatric Sciences, Department of Pediatrics and Department of Biochemistry and Molecular Biology, University of Chicago, 929 East 57th Street, Chicago, IL 60637; and †Department of Physiology, University of Wisconsin, Madison, WI 53706

Contributed by Francisco Bezanilla, March 21, 2007 (sent for review February 28, 2007)

It is now well established that the voltage-sensing S4 segment in voltage-dependent ion channels undergoes a conformational change in response to varying membrane potential. However, the magnitude of the movement of S4 relative to the membrane and the rest of the protein remains controversial. Here, by using histidine scanning mutagenesis in the Shaker K channel, we identified mutants I241H (S1 segment) and I287H (S2 segment) that generate inward currents at hyperpolarized potentials, suggesting that these residues are part of a hydrophobic plug that separates the water-accessible crevices. Additional experiments with substituted cysteine residues showed that, at hyperpolarized potentials, both I241C and I287C can spontaneously form disulphide and metal bridges with R362C, the position of the first charge-carrying residue in S4. These results constrain unambiguously the closed-state positions of the S4 segment with respect to the S1 and S2 segments, which are known to undergo little or no movement during gating. To satisfy these constraints, the S4 segment must undergo an axial rotation of $\approx 180^\circ$ and a transmembrane (vertical) movement of $\approx 6.5 \text{ \AA}$ at the level of R362 in going from the open to the closed state of the channel, moving the gating charge across a focused electric field.

gating current | metal bridge | omega current | S-S bridge

Voltage-gated channels are crucial players in excitability and cell homeostasis. Voltage-dependent sodium and potassium conductances are responsible for the generation and propagation of the nerve impulse (1). The salient property of these channels is the steep membrane potential dependence of their open probability. This voltage dependence is conferred by the voltage sensor that has been identified with their first four transmembrane segments (S1–S4). It is now clear that the four most extracellular basic residues of the S4 segment and the most intracellular acidic residue in the S2 segment in the Shaker K channel are the gating charge-carrying residues that move in the field in response to changes in membrane potential (2, 3). The movement and conformational change of segments S1–S4 within the voltage-sensing module in response to membrane depolarization is somehow coupled to the intracellular gate of the pore domain (S5–S6) to open and close the channel. A multitude of biophysical experiments have attempted to delineate the conformation of the voltage sensor and the position of its charges in the open and closed states. The structural restraints deduced from those experiments have subsequently been shown to be consistent with the overall conformation of the open state from the crystallographic structure of the Kv1.2 channel. However, the experiments providing structural constraints about the closed state conformation of the voltage sensor are more uncertain. Although it is generally accepted that the S1 and S2 helical segments do not move extensively upon gating (4–8), there is disagreement concerning the magnitude of movements associated with the S3 and S4 segments. For example, histidine scanning of the charged residues and cysteine scanning of the S4 and S3 segments indicate that the charges change exposure from

the inside to the outside when the membrane is depolarized (9–13). Notably, the most extracellular arginine residue in the S4 segment of the Shaker K channel (R362) when replaced by histidine produces a proton pore that indicates a very narrow separation between the external and internal solutions in the closed state (10). Consistent with this result, when R362 is replaced with a small amino acid, a cation pore also is generated in the closed state (the omega current) (14, 15). All these results point to the concept of a focused transmembrane electric field, which has been confirmed by an electrochromic probe (16) and by an elegant set of experiments using a variable chain length on the first charge that showed that the separation between the inside and outside is $\approx 4 \text{ \AA}$ (17). The results of fluorescence resonance energy transfer (5, 6) and lanthanide-based resonance energy transfer (4, 7) indicate a limited translocation of the S4 segment across the membrane. Voltage-gating with a limited translocation is physically possible if the transmembrane field is focused because the charged residues of the S4 segment do not need to travel across the entire thickness of the membrane to account for the rather large (13 e) gating charge (18). In contrast to these results, trapping experiments by avidin of site-specific biotinylated channels with the bacterial KvAP channel have suggested a rather large translation of the S4 segment across the membrane (8, 19). The crystal structure of Kv1.2, a eukaryotic potassium channel recently solved (20), is thought to represent the open (inactivated) state based on previously reported biochemical and electrophysiological studies (9, 12, 27, 35). However, despite the accumulating experimental data, the structural constraints providing information about the closed state conformation of the voltage sensor remain scarce and uncertain.

In an attempt to constrain the position of the neighboring helices relative to the voltage-sensing charges in the closed and the open conformation, we initiated a histidine scanning mutagenesis in those segments. This scanning study led us to the detection of two atomic proximity measurements that constrain the positions of the S4 segment with respect to the S1 and S2 segments in the closed state. Using these constraints, the biophysical information available, and the crystal structure of the open state, we present a simplified structural model of the voltage sensor in the closed state. Based on the crystal structure of the open state and this model of the closed state, it is observed that the movements controlling voltage gating mainly involve an axial rotation, a change in tilt, and a transmembrane (vertical) movement of $\approx 6.5 \text{ \AA}$ of the S4 helical segment, resulting into the

Author contributions: F.V.C., B.C., and F.B. designed research; F.V.C. and B.C. performed research; B.R. and F.B. contributed new reagents/analytic tools; F.V.C., B.C., and F.B. analyzed data; F.B. wrote the paper; and B.R. developed the molecular model.

The authors declare no conflict of interest.

*To whom correspondence should be addressed. E-mail: fbezanilla@uchicago.edu.

This article contains supporting information online at www.pnas.org/cgi/content/full/0702638104/DC1.

© 2007 by The National Academy of Sciences of the USA

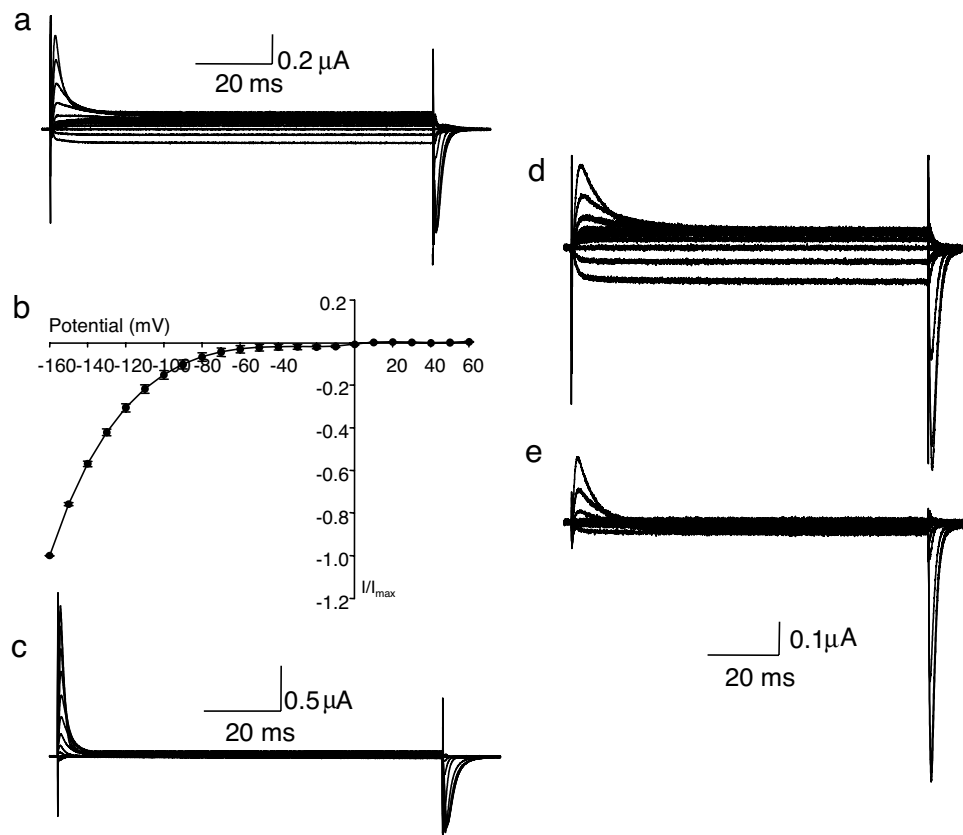


Fig. 1. The proton pore in the I287H mutant. (a) Current family recorded from an oocyte expressing the I287H mutant for a series of pulses from -160 to $+60$ mV in increments of 10 mV. The outside pH value was 5 . (b) Average I - V relationship curve for the proton currents recorded from I287H mutants when the pH value was 5 ($n = 5$). (c) Same oocyte as in a but with outside pH value of 9 . The currents in each potential were normalized to the maximal current. The holding potential was -90 mV and the test pulses (-160 to $+60$ mV) were preceded and followed by a -120 -mV pulse. (d) Current family of another oocyte with an outside pH value of 5 . (e) Same oocyte as in d after external addition of 5 mM Ni^{2+} . Traces shown in d and e were subtracted by using P/4 protocol from a holding potential of $+40$ mV.

translocation of the main gating charge across the focused electric field in the protein core.

Results

Guided by the approximate structural model of Shaker in the closed state presented in a previous study [ref. 5; see also the [supporting information \(SI\)](#)], we replaced several residues in segments other than S4 with histidine residues in an attempt to detect a proton transporter or a proton pore. The logic of this search is that, depending on the membrane potential, if a residue is alternatively exposed to an internally or externally connected water crevice, we should detect a voltage-dependent proton current with a bell-shaped I - V curve, characteristic of a proton transporter (21). On the other hand, if the replaced residue is a barrier between the external and internal water crevice, a proton conductance (formed by a pore mediated through the histidine residue) is observed at either the hyperpolarized or depolarized potential, and its I - V curve should follow the activation of the sensor (9). Several sites in the S1 and S2 segments were tested, and we report here two residues that, when replaced by histidine, generate a proton pore.

I287 in Segment S2 Replaced by a Histidine Generates a Proton Pore at Hyperpolarized Potentials. Fig. 1 shows gating currents from the nonconducting, noninactivating *Shaker-IR-W434F* channel, where I287 has been replaced by a histidine. When the external pH was made acidic (pH 5), an inward current developed at negative potentials (Fig. 1 a and b), and the steady current was

not present at external pH 9 (Fig. 1c). External application of Ni^{2+} blocked the inward current when external pH was 5 (Fig. 1 d and e).

These results indicate that, at negative potentials, I287 is a hydrophobic barrier between the intracellular and extracellular solutions and that, when replaced by histidine, it becomes a proton pore. The proton current of I287H is reminiscent of the proton current recorded when the most extracellular charged residue of S4 is replaced by histidine (R362H) (10). However, the present result does not distinguish whether the two pores are different or happen to block the connection of the solutions in the same part of the protein.

I287 in Segment S2 Contributes to the Hydrophobic Plug in the Closed State. Because I287H, like R362H (10), forms a proton pore in the closed state of the Shaker channel, we posit that these two residues are in close proximity in that conformation and line the same narrow hydrophobic barrier that separates the inside and outside of the cell membrane. To test this hypothesis, we replaced both residues with cysteine. A replacement of R362 with cysteine induces the formation of a cation pore (omega current) (14) that, similar to R362H, also opens at very negative potentials. Most likely, this pore is in the same region of R362H but, because cysteine is a small amino acid that can be negatively charged, it allows cations to pass in that narrow region when the first charge is located in its closed position. If I287 and R362C are in the same region in the closed state, then the cation inward

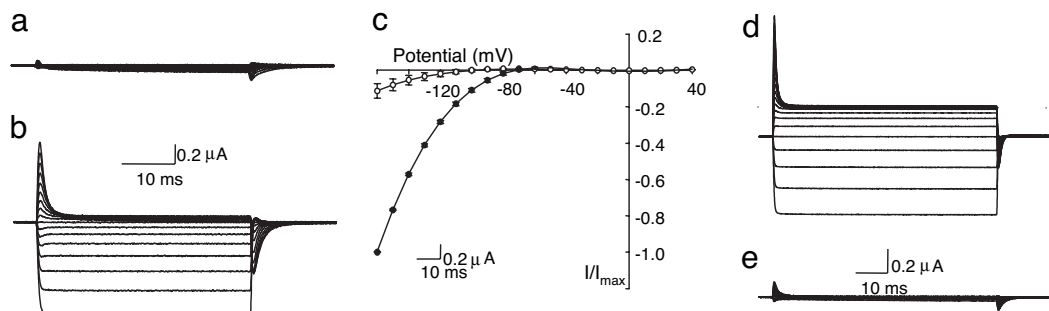


Fig. 2. Effect of DTT and H_2O_2 on I287C-R362C mutant. (a) Currents recorded from an untreated oocyte. (b) Currents from the same oocyte after treatment with 10 mM DTT in the chamber. The holding potential was -90 mV and the 40-ms test pulse varied from -160 to 0 mV ($\text{P}/-4$ subtraction). (c) Average I - V curves measured at the end of 40-ms pulses from oocytes injected with I287C+R362C mutant before (open symbols) and after (filled symbols) treatment with 10 mM DTT ($n = 3$). The currents were normalized by the maximal current recorded after the treatment with DTT. The holding potential was -90 mV , and the test pulses (-160 to $+40\text{ mV}$) were preceded and followed by a -120-mV pulse. (d) Gating and omega currents recorded from an oocyte expressing the I287C+R362C mutant and pretreated with DTT before mounting on the chamber. Dashed line indicates zero membrane current. (d and e) Currents recorded before (d) and after (e) external application of 10 mM H_2O_2 . The records reflect currents elicited by pulses ranging from -160 to $+40\text{ mV}$ with preceding and following pulses of -120 mV (off-line subtraction).

current recorded at negative potentials may still be present when I287 is replaced by a cysteine.

We found that the double mutant I287C+R362C showed no cation or gating currents (experimental traces in Fig. 2a and I - V curve in Fig. 2c) unless DTT is applied externally (experimental traces in Fig. 2b and I - V curve in Fig. 2c), indicating the spontaneous formation of a cysteine bridge between I287C and R362C. Fig. 2d shows the gating current and the omega current from an oocyte injected with the double mutant I287C+R362C that has been pretreated for 2–4 h in 2 mM DTT before being mounted in the cut-open oocyte setup. After external application of H_2O_2 , the gating current and the omega current are blocked, confirming the formation of a bridge between these two cysteine residues (Fig. 2e). There is no effect of H_2O_2 in the WT channel (data not shown). These results suggest that 287C and 362C are indeed in close proximity and that the formation of the proton pore by either R362H or I287H is in the same region. However, it has been shown that two cysteine residues can form bridges even when they are separated by 15 Å, although the rate of formation at those distances is low (22). Because the formation of the bridge is a covalent modification, its formation does not tell us the mechanistic relevance of the proximity unless we were able to measure the rate of formation. For this reason, we tested for the formation of a reversible high-affinity metal bridge using Cd^{2+} that indicates shorter distances.

Fig. 3a shows the currents recorded from an oocyte that has been previously exposed to 2 mM DTT to break the S-S bridge between positions 287C and 362C. The effects of externally adding 1 μM and 100 μM Cd^{2+} are shown in Fig. 3 b and c. It is interesting to note that Cd^{2+} blocks the omega current more effectively than it does the gating current. Fifty percent of the omega current is blocked by 1 μM Cd^{2+} , whereas the gating current is unaffected (Fig. 3b). At 100 μM Cd^{2+} , the omega is almost completely blocked and gating currents are significantly reduced (Fig. 3c). The dose-response curve of the omega current blockade by Cd^{2+} shows micromolar affinity, indicating that 287C and 362C are in close proximity in the closed state of the channel (Fig. 3d, closed circles), whereas it is much higher for the blockade of the gating charge (Fig. 3d, open circles). A simple interpretation of these results is that, upon hyperpolarization, 362C gets very close to 287C, and, when in the presence of Cd^{2+} , these residues form a metal bridge, making an effective plug that interrupts the communication between the inside and outside solutions, thus blocking the omega current. Upon depolarization, the voltage favors the dissociation of Cd^{2+} from the two cysteine residues, allowing the movement of the S4 toward its open position. The dissociation is expected to be favored at low Cd^{2+} concentrations. This result agrees with the fact that the S-S covalent bridge, favored under oxidizing conditions, will block the omega current, but it also will prevent the movement of the

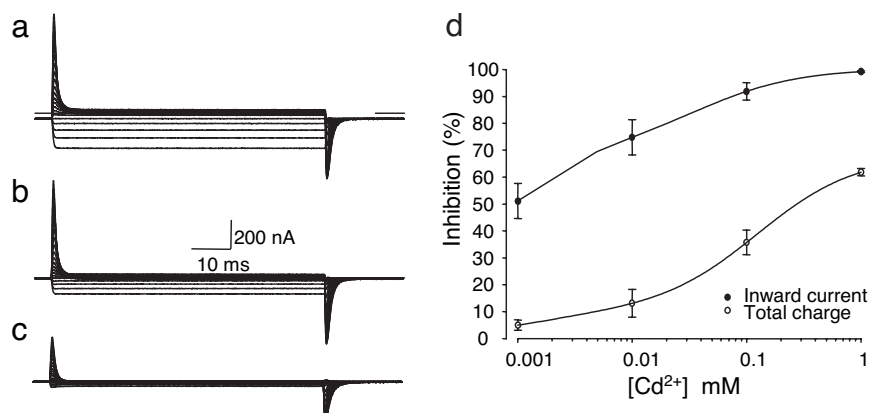


Fig. 3. Effect of external Cd^{2+} on gating and omega currents of the I287C+R362C mutant. Pulses ranged from -160 to $+40\text{ mV}$ in steps of 10 mV. (a) Control recording of an oocyte treated with DTT. (b) Recording after 1 μM Cd^{2+} . (c) Recordings after 100 μM Cd^{2+} . (d) Dose-response curve for the effect of Cd^{2+} on the omega current (filled circles) and the gating charge (open circles).

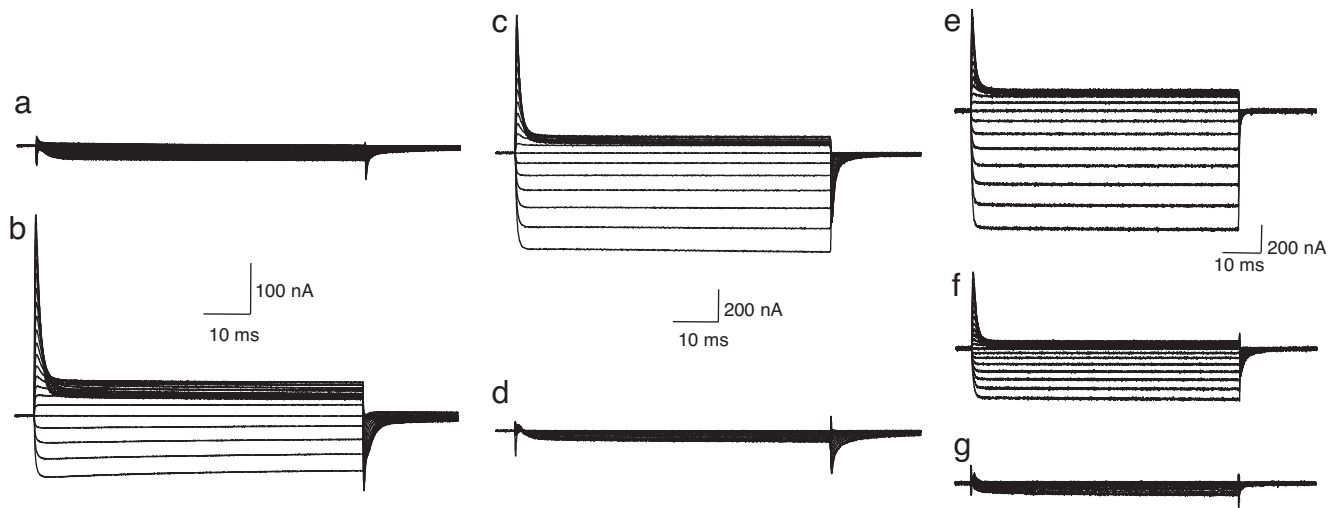


Fig. 4. Recordings from the I241C+R362C mutant. (a) Currents recorded from an untreated oocyte. (b) Currents after treatment with 10 mM DTT in the chamber. (c) Currents from another oocyte that has been treated with 2 mM DTT. (d) Currents after external application of H_2O_2 . (e) Currents from another oocyte that has been treated with DTT. (f) Currents after external application of 1 μM Cd^{2+} . (g) Currents after external application of 100 μM Cd^{2+} . Pulses ranged from -160 mV to $+40$ mV in a, b, and e–g. For traces shown in c and d, pulses from -150 to $+40$ mV were used. For traces shown in c–g, test pulses were not preceded or followed by a -120 -mV pulse.

S4 segment toward its open position, which blocks the gating currents. We conclude from these results that residue 287 and residue 362 approach each other at a close distance, perhaps 6–8 Å in the closed state of the channel. Thus, the proton pore formed by I287H and the proton pore formed by R362H are in the same region and define a constraint on the position of the S4 segment with respect to the S2 segment in the closed state of the channel.

I241 in the S1 Segment Replaced by Histidine Makes a Pore. The second important result from the histidine scanning was the formation of a pore in position 241 when replaced by histidine. We found that oocytes injected with the Shaker-IR-W434F with the I241H mutation died 2 days after injection. Our attempts at recording currents in those early days were unsuccessful because the oocytes showed high leak. We then incubated the oocytes at 12°C to allow the synthesis of the protein but preventing their insertion on the plasma membrane. Under these conditions, the oocytes survived until the temperature was raised, indicating that the damage was due to the insertion of the channels on the membrane. In some cases, just after raising the temperature we were able to record large inward currents at negative potentials, similar to the currents observed for the I287H mutant (see the SI). This suggested the possibility that I241 in the S1 segment also was involved in the region of the proton pore observed for R362H and I287H, as described above.

I241 in Segment S1 Contributes to the Hydrophobic Plug in the Closed State. We then proceeded to replace I241 with cysteine and A362 with cysteine. This double mutant did not deteriorate the oocytes; in fact, we found, as was the case with the R362C+I287C mutant, that the omega current and the gating current were completely blocked when the oocyte was tested in the cut-open oocyte chamber. Fig. 4a shows the virtual absence of gating and omega currents recorded from an oocyte that was not pretreated with DTT. Robust gating and omega currents appeared as soon as the oocyte was treated with 10 mM DTT in the chamber under voltage clamp (Fig. 4b). If the oocyte were pretreated with DTT before being mounted in the chamber, large omega and gating currents were recorded (Fig. 4c). The addition of 10 mM H_2O_2 blocked both the omega and the gating

currents (Fig. 4d). The proximity between residues was tested again by adding Cd^{2+} to the external solution, as was done for the R362C+I287C mutant. As before, addition of Cd^{2+} blocked the omega current more effectively than it did the gating current. Fig. 4e shows the omega current and gating currents after DTT treatment. The addition of 1 μM Cd^{2+} blocked half of the omega current and had no effect on the gating currents (Fig. 4f), whereas the addition of 100 μM Cd^{2+} blocked both currents (Fig. 4g). The dose-response curve is shown in the SI. The effect of Cd^{2+} and the spontaneous formation of the covalent bond indicate that residues 241C and 362C approach closely in the closed state. We conclude from these results that the pore formed in the closed state near the first charged residue (R362) is formed in a region that includes position I241 in the S1 segment and I287 in the S2 segment.

Other Residues in the Region of the Ion Pore in the Closed Position. It is interesting to note that in the WT Shaker position 286 in segment S2 is a cysteine residue. Although this position is only one residue apart from the position (I287C) that spontaneously forms the cysteine bridge with R362C, native C286 does not form such a bridge spontaneously. In the single mutant R362C, adding H_2O_2 did block the inward omega current with no effect on the gating currents (see the SI), indicating that R362C and C286 do not form a covalent S-S bridge. In a detailed study of the reaction between cysteine and H_2O_2 (23), it was found that, if there were an excess of H_2O_2 with respect to cysteine, the reaction proceeds from cysteine sulfenic acid to cysteine sulfenic acid and finally to cysteine sulfonic acid ($\text{Cys}-\text{SO}_3\text{H}$). In our case, if the two cysteine residues were not in the correct orientation or distance to form the bridge, it would be equivalent to having an excess of H_2O_2 and we would favor the formation of cysteine sulfonic acid. This compound is more bulky than cysteine and may explain the block of the ionic current upon hyperpolarization. In addition, external Cd^{2+} blocks the inward omega current in the single mutant (R362C) but has no effect on the gating currents at low concentrations. This result could be due to the bulk introduced by Cd^{2+} that could be stabilized by the field and attached to R362C, C286, or E283 or a combination of these three residues.

Discussion

The histidine scanning of residues within segments S1 and S2 pointed to two positions (I241H in segment S1 and I287H in segment S2) that generate a current at negative potentials, thus playing an important role in insulating the external solution from the internal solution. These positions were explored in more detail in an attempt to locate them with respect to the current induced by the replacement of the first most extracellular charge (R362) with histidine or cysteine, which also generates a current at negative potentials. The spontaneous formation of cysteine bridges by I241C with R362C as well as I287C with R362C indicated that these conduction pores are in the same region of the protein. These results help delineate the narrow region that separates the extracellular solution from the intracellular solution in the closed state of the WT channel. We propose that, in the closed state of the voltage sensor, the electric field is focused across a dielectric hydrophobic plug formed by the methylene groups of A362 in segment S4 together with those of I241 in segment S1 and I287 in segment S2. Making those chains less bulky and more hydrophilic establishes a direct communication between the external and internal solutions when the sensor is moved into its closed state by hyperpolarization.

Minimal Model of the Voltage Sensor and Pore Opening. With the structural constraints presented here, we have built a simplified model of the position of segment S4 in the closed state of the channel by using the crystal structure of the open (inactivated) state of Kv1.2 as a starting point. By choice, the model was kept as simple as possible to keep the number of assumptions to a minimum and to make our conclusions unambiguous.

Assumption 1. The position of segment S4 in the model is constrained by the results presented here, such that R362 (in segment S4), I241 (in segment S1), and I287 (in segment S2) are in atomic proximity in the closed state, and by the necessity to keep the connection with the S4–S5 linker in contact with the C terminus of the S6-helix of the closed intracellular gate.

Assumption 2. The intracellular gate is constructed according to the data of the Yellen laboratory (24–27), which shows that cysteine side chains in the Shaker mutant V478C remain accessible to a series of fairly large reagents and that a high-affinity Cd²⁺ binding site can be reached in the closed state. The closed gate formed by straight α -helices as observed in the x-ray structure of the KcsA channel is not compatible with these observations because the corresponding position is located deep within the narrow helical bundle crossing and would not be accessible from the intracellular side by large reagents or by Cd²⁺. The model for the closed gate was constructed to keep the V478 site accessible to the intracellular side by treating the conserved PVP motif in S6 as a hinge between two semirigid helical parts. The model was obtained by refining the geometry while imposing a distance of $\approx 5 \text{ \AA}$ to a Cd²⁺ bound to V478C. Only the residues in the PVP region were allowed to move, whereas the C terminus of S6 moved as a rigid body. The S4–S5 linker was then translated rigidly to preserve exactly its orientation with respect to the S6 position as in the crystal structure of Kv1.2.

Assumption 3. The S1 and S2 segments do not move between the closed and open state. Although there is some movement of segments S1 and S2 in a more refined model of the closed state,[§] this assumption is consistent with the small movement detected by luminescence resonance energy transfer on Shaker (4, 7) and by biotin-avidin trapping experiments on KvAP (8).

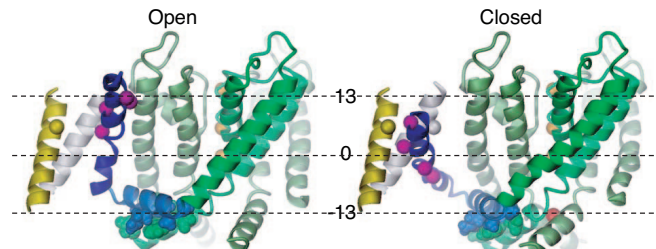


Fig. 5. Minimal model of a Kv channel in its open and closed state. Only one voltage sensor and three subunits of the pore domain are shown for clarity. Segments S1 (white), S2 (yellow), and S4 (blue); the S4-S5 linker (slate blue); S6–S6 (green); and K⁺ ions (orange) are shown. The C β of the four gating charge of segment S4 (residues 362, 365, 368, and 371) are shown (magenta) together with the C β of I241 in segment S1 (white) and I287 in segment S2 (yellow). For the closed state, a Cd²⁺ (red) is placed where it would bind the cysteine residue of the V478C Shaker mutant. The dashed lines respectively indicate the center of the membrane and the membrane–solution interface at 0 Å and $\pm 13 \text{ \AA}$.

Assumption 4. The movement of S4 consists in a simple rigid body rotation and translation of residues 358–378 (keeping the helix as in the crystal structure).

Simultaneously satisfying all of the constraints on segment S4 under those conditions necessitates an S4-helix rotation of $\approx 180^\circ$ around its axis, a change in tilt, and a vertical translation of $\approx 6.5 \text{ \AA}$ toward the intracellular side. In the “down” state of segment S4, the first gating charge R362 is within $\approx 7 \text{ \AA}$ from both I241 and I287 (C β –C β distances), where it is located at the center of the outer leaflet of the bilayer membrane, $\approx 6.5 \text{ \AA}$ away from the extracellular aqueous solution. The minimal model is illustrated in Fig. 5; consistency with a refined model of the complete Kv1.2 channel[§] is shown in the SI.

The minimal model of the closed state presented here agrees with a large body of literature. The presence of a narrow hydrophobic region enclosed between segments S1, S2, and S4 is consistent with the data that proposes a focused field in this region (10, 16, 17). This finding is, in turn, consistent with a small movement of the S4 segment resulting in the translocation of four charged residues per subunit in the narrowed focused field. The luminescence resonance energy transfer measurements between the toxin and the S4 segment indicate a small change of $\approx 1 \text{ \AA}$ (7). In the model proposed here, the translation perpendicular to the membrane is $\approx 6.5 \text{ \AA}$, which is consistent with the luminescence resonance energy transfer measurements if one considers the flexibility of the tethered fluorophores (7) and the flexibility of the voltage sensor (V. Jogini and B.R., unpublished data). In the model, the first two charges move in the extracellular half of the lipid bilayer, which is consistent with the FRET results obtained with dipicrylamine in the lipid bilayer and tetramethylrhodamine and ABD dyes in the S4 segment. In these experiments, the fluorescence signal from labels attached as deep as position 367 in segment S4 did not show the transient component that would be expected if the labeled sites were to cross the middle of the bilayer (5). The minimal model also agrees with the recent data on the omega current (15). In this model, we have not explicitly included the S3 segment because our data does not address its position directly. Possible movements and constraints of segment S3 movement with respect to segment S4 have been studied by Gonzalez *et al.* (28, 29) in shorter S3–S4 linker constructs and in accessibility studies.

The results and the model presented here makes it clear that the first two basic residues in segment S4 (R362 and R365) are pointing toward S1–S3 in the down state, whereas the next two basic residues (R368 and R371) are exposed to the large aqueous crevice on the intracellular side. In the open state, R362 and

[§]Yarov-Yarovoy, V. M., Roux, B., Jogini, V., Tombola, F., Pathak, M. M., Isacoff, E. Y. (2007) Biophys Soc Abstr, in press (abstr.).

R365 are near the membrane solution interface, whereas R368 and R371 are making salt bridges with acidic residues of S2 and S3. Therefore, no charge is ever exposed directly to the lipid hydrocarbon region in the open state or in the closed state.

Residues of the Hydrophobic Plug in the Open State. In our modeling we have assumed that the open state is exactly as shown in the crystal structure of Kv1.2. In this structure, the fourth charge (R371) is in close proximity to I287 and I241. When position 371 is replaced by histidine, a proton current is observed that can be interpreted as a combination of a transporter and a pore or just a proton pore (9). Molecular dynamic simulations of Kv1.2 show that water penetrates into the protein but is excluded from the region where the fourth charge resides, consistent with the idea that the fourth charge resides in the position of the hydrophobic plug (ref. 30 and V. Jogini and B.R., unpublished data). A prediction of the Kv1.2 structure is that R371C and I287C should form a covalent bridge in the open state. Accordingly, we have tested this double mutant and found that such a bridge does not form spontaneously (see the SI). Although a negative result in the formation of a cysteine–cysteine bridge cannot be used to show that the two residues are not in proximity, there is still the possibility that they are indeed not close enough and that the crystal structure is not exactly representative of the open state. Because the Kv1.2 crystal was obtained in the absence of membrane potential, the channel is expected to have stabilized in the slow inactivated state. Gating currents measurements have shown that the voltage dependence of the charge vs. potential curve shifts by ≈50 mV to more negative potentials when the channel is inactivated (31), indicating that the voltage sensor changes its conformation when going from the open to the inactivated state. Further experiments that take into account the open and open-inactivated states will be required to resolve in detail the position of the voltage-sensing residues in the open state.

Methods

Mutagenesis and Expression of Channels. The nonconducting (W434F) (32), noninactivating (IR Δ6–46) (33) *Shaker* potas-

sium channel was used as the background template for all of the mutagenesis. All of the mutagenic fragments generated by PCR were sequenced. The RNA was transcribed from the NotI-linearized DNA clone (New England Biolabs, Ipswich, MA) by using T7 RNA polymerase (Ambion, Austin, TX), and 50 nl of 0.5–1 μ g/ μ l RNA was injected into *Xenopus* oocytes. After injection, the oocytes were incubated at 18°C (unless otherwise stated) in an incubation solution containing 96 mM NaCl, 2 mM KCl, 1 mM MgCl₂, 1.8 mM CaCl₂, and 5 mM Hepes, pH 7.3.

Electrophysiology. Ionic and gating currents were measured 2–4 days after injection. Currents were recorded at room temperature (\approx 20°C) with the cut-open oocyte voltage clamp technique (34). The external recording solutions for the histidine scanning experiments contained 176 mM Tris, 44 mM CHES, and 2 mM CaCl₂, pH 9, and 21 mM Tris, 246 mM Mes, and 2 mM CaCl₂, pH 5. The internal solutions contained 176 mM Tris, 44 mM CHES, and 2 mM EGTA, pH 9, and 17 mM Tris, 246 mM methylsulfonate, and 2 mM EGTA, pH 5. For the cysteine substitution experiments, the external solution contained 115 mM N-methyl-D-glucamine-Mes, 20 mM Hepes, and 2 mM Ca-Mes, pH 7.4. The internal solution was the same as the external solution, except that Ca-Mes was replaced by EGTA-N-methyl-D-glucamine. There was no subtraction or compensation of leak components during the acquisition (unless otherwise stated); the subtraction was done off-line. The data were filtered at 5 kHz and sampled at 50 kHz. The currents were measured from a holding potential of –90 mV in response to various test potentials, preceded and followed by a –120 mV pulse (unless otherwise stated). Test pulses were at least 40 ms long and were applied with a 2-s interval. Data acquisition and analysis were carried out with in-house programs.

We are grateful to Vladimir Yarov-Yarovoy for helpful discussions and for sharing the coordinates of the closed-state model of Kv1.2 (shown in SI) submitted as an abstract to the Biophysical Society. This work was supported by National Institutes of Health Grant GM30376. B.C. was supported by the Scientist Development Fund from the American Heart Association. B.R. was supported by National Institutes of Health Grant GM062342.

1. Hodgkin AL, Huxley AF (1952) *J Physiol* 117:500–544.
2. Aggarwal SK, MacKinnon R (1996) *Neuron* 16:1169–1177.
3. Seoh S-A, Sigg D, Papazian DM, Bezanilla F (1996) *Neuron* 16:1159–1167.
4. Cha A, Snyder G, Selvin PR, Bezanilla F (1999) *Nature* 402:809–813.
5. Chanda B, Asamoah OK, Blunck R, Roux B, Bezanilla F (2005) *Nature* 436:852–856.
6. Glauner KS, Mannuzzu LM, Gandhi CS, Isacoff EY (1999) *Nature* 402:813–817.
7. Posson DJ, Ge P, Miller C, Bezanilla F, Selvin PR (2005) *Nature* 436:848–851.
8. Ruta V, Chen J, MacKinnon R (2005) *Cell* 123:463–475.
9. Starace DM, Bezanilla F (2001) *J Gen Physiol* 117:469–49017.
10. Starace DM, Bezanilla F (2004) *Nature* 427:548–552.
11. Baker OS, Larsson HP, Mannuzzu LM, Isacoff EY (1998) *Neuron* 20:1283–1294.
12. Larsson HP, Baker OS, Dhillon DS, Isacoff EY (1996) *Neuron* 16:387–397.
13. Yang N, Horn R (1995) *Neuron* 15:213–218.
14. Tombola F, Pathak MM, Isacoff EY (2005) *Neuron* 45:379–388.
15. Tombola F, Pathak MM, Gorostiza P, Isacoff EY (2006) *Nature* 445:546–549.
16. Asamoah OK, Wuskell JP, Loew LM, Bezanilla F (2003) *Neuron* 37:85–97.
17. Ahern CA, Horn R (2005) *Neuron* 48:25–29.
18. Schoppa NE, McCormack K, Tanouye MA, Sigworth FJ (1992) *Science* 255:1712–1715.
19. Jiang Y, Ruta V, Chen J, Lee A, MacKinnon R (2003) *Nature* 423:42–48.
20. Long SB, Campbell EB, MacKinnon R (2005) *Science* 309:897–903.
21. Starace DM, Stefani E, Bezanilla F (1997) *Neuron* 19:1319–1327.
22. Careaga CL, Falke JJ (1992) *J Mol Biol* 226:1219–1235.
23. Luo D, Smith SW, Anderson B (2005) *J Pharm Sci* 94:304–316.
24. del Camino D, Yellen G (2001) *Neuron* 32:649–656.
25. Holmgren M, Shin KS, Yellen G (1998) *Neuron* 21:617–621.
26. Holmgren M, Yellen G (1998) *Biophys J* 74:A254.
27. Webster SM, Del Camino D, Dekker JP, Yellen G (2004) *Nature* 428:864–868.
28. Gonzalez C, Roseman E, Bezanilla F, Alvarez O, Latorre R (2001) *Proc Natl Acad Sci USA* 98:9617–9623.
29. Gonzalez C, Morera FJ, Rosenmann E, Alvarez O, Latorre R (2005) *Proc Natl Acad Sci USA* 102:5020–5025.
30. Treptow W, Tarek M (2006) *Biophys J* 90:L64–L66.
31. Olcese R, Latorre R, Toro T, Bezanilla F, Stefani E (1997) *J Gen Physiol* 110:579–590.
32. Perozo E, MacKinnon R, Bezanilla F, Stefani E (1993) *Neuron* 11:353–358.
33. Hoshi T, Zagotta WN, Aldrich RW (1990) *Science* 250:533–538.
34. Stefani E, Bezanilla F (1998) *Methods Enzymol* 293:300–318.
35. Sprunger LK, Stewig NJ, O'Grady SM (1996) *Eur J Pharmacol* 314:357–364.